

Engineering Model to Predict Behaviors of Shape Memory Alloy Wire for Vibration Applications

M.K. Kang¹, E.H. Kim¹, M.S. Rim¹ and I. Lee^{1,2}

Abstract: An engineering model for predicting the behavior of shape memory alloy (SMA) wire is presented in this study. Piecewise linear relations between stress and strain at a given temperature are assumed and the mixture rule of Reuss bounds is applied to get the elastic modulus of the SMAs in the mixed phase. Critical stresses and strains of the start and finish of the phase transformation are calculated at a given temperature by means of a linear constitutive equation and a stress-temperature diagram. Transformation conditions based on the critical stresses are translated in terms of critical strains. Martensite volume fraction and stress at the end of the increment are calculated using the defined linear transformation path by algebraic manner. To consider the trained behavior and strain rate dependent behavior of SMA wire, model correlation with the experimental data was made for specific SMA material. A numerical example of vibration response of the SMA wire damped beam is presented to demonstrate the strain dependent behavior. System damping capacity is reduced by considering fast strain rate loading compared to the case of counting the quasi-static behavior of SMA wire.

Keywords: Shape memory alloy, Phase transformation, Training, Strain rate.

1 Introduction

Shape memory alloys (SMAs) are smart materials that are of interest to engineers because they can undergo large strain and can have extremely high recovery stress when they are heated.

NiTi (nitinol) is a commercial SMA which is widely used and researched in the field of aerospace engineering and architectural engineering as an actuating or damping material because of its shape memory effect and superelastic effect [Birman (1997); Saadat, Noori, Davoodi, Hou, Suzuki and Masuda (2001)]. Moreover, plentiful

¹ School of Mechanical, Aerospace and Systems Engineering, KAIST, Daejeon, Republic of Korea

² Corresponding Author: I. Lee, E-mail: inlee@kaist.ac.kr

medical applications of surgical devices made using NiTi are in use due to its biocompatibility and anti-corrosion properties [Pelton, Stöckel and Duerig (2000)]. Recently, it has become common to find products such as mobile phone antennas and shape memory eyeglasses nearby ourselves made using SMAs.

SMA material is applied to actuators not only for active control but also for passive control [Rogers (1990); Dolce, Cardone and Marnetto (2000)]. For use in an active control device, temperature control of the SMA material is mandatory. For use in a passive control device, the operating temperatures and mechanical environments of the SMA should be defined clearly when designing the control device.

Many models simulating the thermo-mechanical behaviors of SMAs have been introduced. Among them, the models of Tanaka, Liang, Brinson and Lagoudas are well known and have been verified by many other researchers. Many applications and reproductions have been made based on their models [Tanaka, Kobayashi and Sato (1986); Liang, Rogers (1990); Brinson (1993); Qidwai and Lagoudas (2000)]. Recent models have tended to prescribe details of various behaviors of SMAs and to become more complicated and sophisticated, making it more difficult for engineers to apply such models when designing their applications. For this reason, the models of Liang and Brinson are often preferred as relatively easy to implement. However, when these models are used without any modification, unique behaviors of SMAs such as trained stress-strain response due to cyclic loads and strain rate dependent response cannot be simulated properly.

Prahlad and Chopra (2003) used time dependent kinetics together with the constitutive equation in the rate form to simulate strain rate dependent behavior, and iterative methods are selected to solve the simultaneous partial differential equations. This approach requires increased computation costs and greater efforts are required to solve the equations. Quidwai and Lagoudas (2000) pointed out that numerical convergence may fail or convergence speed may slow down around the end of transformation. They recommended two remedies for resolving these problems in numerical simulation using their own model. Lagoudas, Ravi-Chandar, Sarh and Popov (2003) showed that the computational costs are notably increased when the strain rate dependent model is used together with general fixed mesh system in the finite element method.

In the design stage, there can be the need for simpler models which capture physical characteristics of the material behavior, even if other models with high fidelity are already in place, for the reasons of reducing computational cost and modeling complexity. Sometimes, a simple and easy model with the minimum input parameters is preferred to check the overall tendency of the objects being designed within a short time. According to NiTi wire tests results, the nearly linear behavior between stress and strain is often observed during phase transformation. Therefore,

dramatic model simplification could be achieved using linear equations and a time independent constitutive equation to simulate the macroscopic phenomenological behavior of the SMA. For example, Lagoudas, Mayes and Khan (2001) introduced a simplified model for the purpose of analyzing the vibration response of SMA material. When they compared the simplified model with the energy based model [Quidwai and Lagoudas (2000)], the computation time of the simplified model was only one seventh that of the energy based model to achieve nearly the same results. SMAs exhibit different behaviors after cyclic loading than when in the virgin state. The more cycles are applied, the more irreversible strains accrue. As the number of cycles is increased, plateau stress is decreased. Ren, Li and Song (2007) included these phenomena to a simplified model in an experimental context, and a stable superelastic behavior was achieved after 30 cyclic loads.

The stress-strain behavior of SMAs under a quasi-static loading condition is different from that under high strain rate loading. Tobushi, Shimeno, Hachisuka and Tanaka (1998) researched strain rate dependent behavior by tensile tests under various strain rates. Dolce and Cardone (2001) pointed out that latent heat caused by phase transformation affects phase transformation itself as well as the damping capacity of SMAs. The exothermic and endothermic nature of crystallographic phase transformation changes the temperature of the material. Some portion of the latent heat caused by mechanical loads moves to the surroundings, and this movement of heat can be affected by configuration related and environmental factors such as the shape of the SMA, the surrounding medium, the ambient temperature and so on [Prahlad and Chopra (2003)]. Motahari and Ghassemieh (2007) considered a multi-linear SMA model in which they regarded the very high strain rate loading process as an adiabatic process.

In this paper, we introduce a SMA wire model for engineering that includes strain rate dependent behavior and we demonstrate the application of this model. Simplified superelastic behavior is modeled here based on the assumption of linear relations between stress and strain. Martensite volume fraction is used as an internal parameter indicating the material state and a phase transformation kinetic is constructed for the forward transformation and the reverse transformation. Distinctive routines of major-loop and sub-loop are merged into the transformation kinetic and all conditions for transformations are described in terms of strain since we have assumed linear relations between stress and strain. The mixture rule of Reuss bounds is selected to obtain the material property of the SMA in the mixed phase, which returns a unique martensite volume fraction for the given stress and strain value at a constant temperature. Training effects can also be included by using stabilized material properties obtained through a cyclic process while neglecting irreversible strain.

2 Quasi-static Iso-thermal Engineering Model

A Figure 1 shows a critical stress and temperature phase diagram. The information in this diagram can be obtained using Differential Scanning Calorimeter (DSC) test and several tensile tests under isothermal conditions at various temperatures [Prahlad and Chopra (2001)]. Figure 2 shows an idealized superelastic behavior in the stress and strain space.

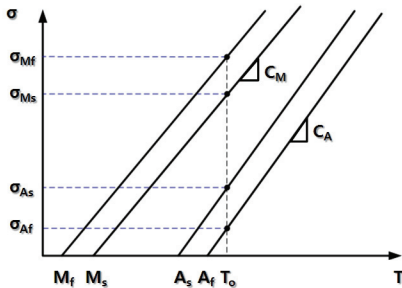


Figure 1: Critical stress - temperature diagram

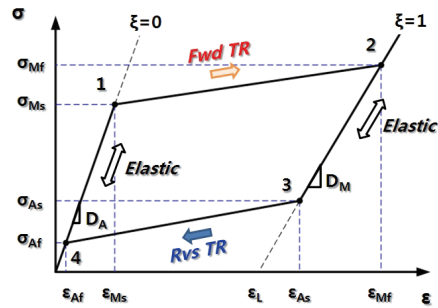


Figure 2: Idealized superelastic behavior

Where ‘ σ ’ is stress, ‘ T_o ’ is constant temperature. ‘ C ’ represents the slope of the line in Figure 1 and ‘ D ’ represents the elastic modulus. ‘ A ’ stands for austenite, ‘ M ’ stands for martensite, ‘ s ’ stands for start, and ‘ f ’ stands for finish. ‘ M_s ’ and ‘ M_f ’ are the martensite start temperature and martensite finish temperature, respectively. ‘ A_s ’ and ‘ A_f ’ are the austenite start temperature and austenite finish temperature.

In classical plasticity, Total strain is often additively decomposed into elastic strain (ϵ_{el}) and plastic strain. In the proposed model, transformation strain (ϵ_{tr}) is used instead of plastic strain:

$$\epsilon = \epsilon_{el} + \epsilon_{tr}. \tag{1}$$

Transformation strain describes the quantity deformed due to phase transformation and depends on the crystallographic material state. Transformation strain can be written as:

$$\epsilon_{tr} = \xi \epsilon_L \quad (0 \leq \xi \leq 1), \tag{2}$$

where ξ is the martensite volume fraction that represents the percentage of the material transformed to martensite phase. ϵ_L is the maximum transformation strain

in the axial direction. It is assumed that all of the crystallographic structure of the material is austenite phase in the case of $\xi = 0$ and martensite phase in the case of $\xi = 1$.

Considering the Gibbs free energy and thermodynamic laws, the constitutive equation is derived as follows [Motahari and Ghassemieh (2007)]:

$$\sigma = D(\xi)[\varepsilon - \alpha(\xi)(T - T_o) - \xi \varepsilon_L]. \quad (3)$$

For iso-thermal process ($T = T_o$), thermal expansion can be neglected and Equation (3) gives:

$$\sigma = D(\xi)\varepsilon_{el} = D(\xi)(\varepsilon - \xi \varepsilon_L), \quad (4)$$

where $D(\xi)$ is the elastic modulus in the mixed phase and depends on the martensite volume fraction. It is assumed that the material obeys the mixture rule of the Reuss bound:

$$D(\xi) = \frac{D_M D_A}{\xi(D_A - D_M) + D_M} \quad (5)$$

where D_A , D_M are the elastic moduli of the material in the fully austenite phase and in the fully martensite phase, respectively.

From Equations (4) and (5), the martensite volume fraction can be expressed to have a unique value for the given stress-strain state as follows:

$$\xi = \frac{D_A D_M \varepsilon - D_M \sigma}{D_A D_M \varepsilon_L + (D_A - D_M) \sigma}. \quad (6)$$

2.1 Superelastic behavior

2.1.1 Critical stresses

In the engineering model, stress-strain relations during transformations are assumed as linear. It is also assumed that forward transformation starts when the stress exceeds the martensite start stress (σ_{Ms}) during the loading process ($dE > 0$) and that reverse transformation starts when the stress level during unloading ($dE < 0$) reduces to a level lower than that of austenite start stress (σ_{As}).

Critical stresses (σ_{crit}) in Figure 1 can be written in the following form:

$$\sigma_{crit} = C_x(T - T_x), \quad (7)$$

where ' T_x ' stands for the transformation start or finish temperatures. ' C_x ' stands for the slopes of the transformation bands. Critical stresses for $T = T_o$ ($T_o > A_f$) are

obtained as follows, and correspond to points 1 through 4 in Figure 2

$$\begin{aligned}
 \sigma_{Ms} &= C_M(T_o - M_s) = S_1, \\
 \sigma_{Mf} &= C_M(T_o - M_f) = S_2, \\
 \sigma_{As} &= C_A(T_o - A_s) = S_3, \\
 \sigma_{Af} &= C_A(T_o - A_f) = S_4.
 \end{aligned}
 \tag{8}$$

Critical strains are

$$\begin{aligned}
 \epsilon_{Ms} &= \sigma_{Ms}/D_A = E_1, \\
 \epsilon_{Mf} &= \sigma_{Mf}/D_M + \epsilon_L = E_2, \\
 \epsilon_{As} &= \sigma_{As}/D_M + \epsilon_L = E_3, \\
 \epsilon_{Af} &= \sigma_{Af}/D_A = E_4.
 \end{aligned}
 \tag{9}$$

The constitutive equation (Equation (4)) should be satisfied if there is no phase transformation. When the loading process ends before the completion of transformation and the unloading process starts, there is no transformation until the stress drops to the austenite start stress. Figure 3 shows stress-strain behavior for SMA in the mixed phase. When the material is in the mixed phase, segment 5-2 is selected as the forward transformation path and segment 6-4 is selected as the reverse transformation path since we have assumed a linear stress-strain relation during transformation.

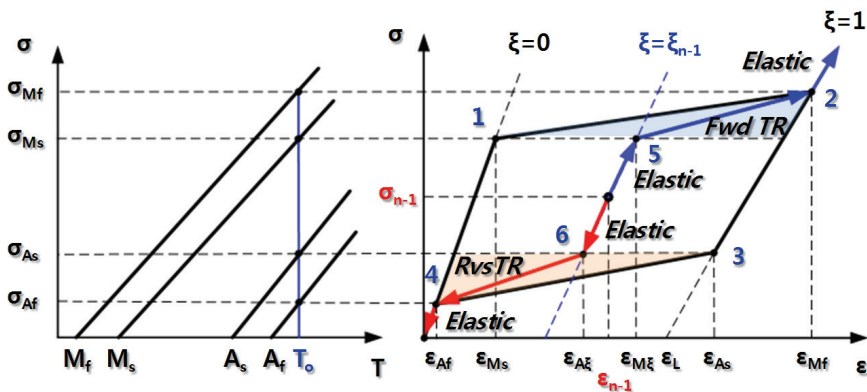


Figure 3: Modeling of superelastic behavior

If we define the increment start position as ‘ $n - 1$ ’ and the increment finish position as ‘ n ’ during nonlinear analysis, the stress (S_n) and martensite volume fraction (ξ_n)

at the increment finish position can be calculated for the given strain increment using the values at the increment start position.

Points 5 and 6 in Figure 3 are determined according to the value of the martensite volume fraction at the increment start position.

$$\begin{aligned} \varepsilon_{M\xi} &= \sigma_{Ms}/D(\xi_{n-1}) + \xi_{n-1}\varepsilon_L = E_5(\xi_{n-1}) \\ \varepsilon_{A\xi} &= \sigma_{As}/D(\xi_{n-1}) + \xi_{n-1}\varepsilon_L = E_6(\xi_{n-1}) \end{aligned} \quad (10)$$

2.1.2 Forward Transformation ($dE > 0$, $E_{M\xi} < E_n < E_{Mf}$):

Most researchers have used stress and temperature as control variables. Researchers pursuing this strategy have had to find the corresponding stress first to check whether the transformation would occur, since the strain is generally determined first when using the finite element method. Jaber, Smaoui and Terriault (2008) proposed an SMA beam model based on the finite strain description, in which a modified stress-strain phase diagram is introduced to describe phase transformations in terms of finite strain. Although it is natural that phase transformation start and finish conditions depend on the critical stress, it is possible to express criteria in terms of strains directly, since we have assumed piecewise linear relations between stress and strain.

Segments 1-2($\xi_{n-1} = 0$) and 5-2($0 < \xi_{n-1} < 1$) are the forward transformation paths. The stresses in these segments are determined by the strain at the increment finish position:

$$S_n = S_2 + \frac{S_2 - S_k}{E_2 - E_k}(E_n - E_2), \quad (11)$$

where

$$S_k = \begin{cases} S_{n-1} & (E_{n-1} \geq E_{M\xi}) \\ S_{M\xi} & (E_{n-1} < E_{M\xi}) \end{cases},$$

$$E_k = \begin{cases} E_{n-1} & (E_{n-1} \geq E_{M\xi}) \\ E_{M\xi} & (E_{n-1} < E_{M\xi}) \end{cases}.$$

The martensite volume fraction is calculated from Equation (6):

$$\xi_n = \frac{D_A D_M E_n - D_M S_n}{(D_A - D_M) S_n - D_A D_M \varepsilon_L}. \quad (12)$$

2.1.3 2.1.3. Reverse Transformation ($dE < 0$, $E_{Af} < E_n < E_{A\xi}$)

Segments 3-4 ($\xi_{n-1} = 1$) and 6-4 ($0 < \xi_{n-1} < 1$) are the reverse transformation paths. Similarly,

$$S_n = S_4 + \frac{S_k - S_4}{E_k - E_4} (E_n - E_4), \tag{13}$$

where

$$S_k = \begin{cases} S_{n-1} & (E_{n-1} \leq E_{A\xi}) \\ S_{M\xi} & (E_{n-1} > E_{A\xi}) \end{cases},$$

$$E_k = \begin{cases} E_{n-1} & (E_{n-1} \leq E_{A\xi}) \\ E_{M\xi} & (E_{n-1} > E_{A\xi}) \end{cases}.$$

The martensite volume fraction is calculated by Equation (12).

2.1.4 Elastic Behavior ($dE = 0$ or $E_{A\xi} < E_n < E_{M\xi}$ or $E_n \leq E_{Af}$ or $E_n \geq E_{Mf}$)

In the segments corresponding to elastic regions, no more transformation occurs. Therefore, the martensite volume fraction can be determined first and then stress can be calculated using the martensite volume fraction at the increment finish position.

$$\xi_n = \begin{cases} \xi_{n-1} & (E_{A\xi} \leq E_n \leq E_{M\xi}) \\ 1 & (E_n \geq E_{Mf}) \\ 0 & (E_n \leq E_{Af}) \end{cases},$$

$$S_n = \begin{cases} D(\xi_n)(E_n - \xi_n \epsilon_L) & (E_n \geq 0) \\ 0 & (E_n < 0) \end{cases}. \tag{14}$$

Experimental research on SMA has discovered asymmetric behavior in its tension and compression [Liu, Xie, Humbeeck and Delaey (1998)]. Since SMA wire cannot sustain compression, stress and martensite volume fraction are set as zero for $E_n \leq 0$.

In the nonlinear analysis, a tangent stiffness computation is required. If the transformation occurs for the given strain increment, the slope of the transformation path becomes the tangent stiffness. For elastic regions, the elastic modulus becomes the tangent stiffness.

2.2 Trained Behavior of SMA

Irreversible residual strain increases and plateau stresses decrease with cyclic loads [Tobushi, Shimeno, Hachisuka and Tanaka (1998)]. The magnitude of the residual strain due to cyclic load depends on the magnitude of maximum training strain and the number of cyclic loads [Wang, Xu and Yue (2008)]. Plateau stresses decrease exponentially and approach a stable response as cycles repeat [Ren, Li and Song (2007)]. Therefore, a training process should precede actual use of the SMA in application. The behavior of trained SMA can be simplified and modeled as in Figure 4.

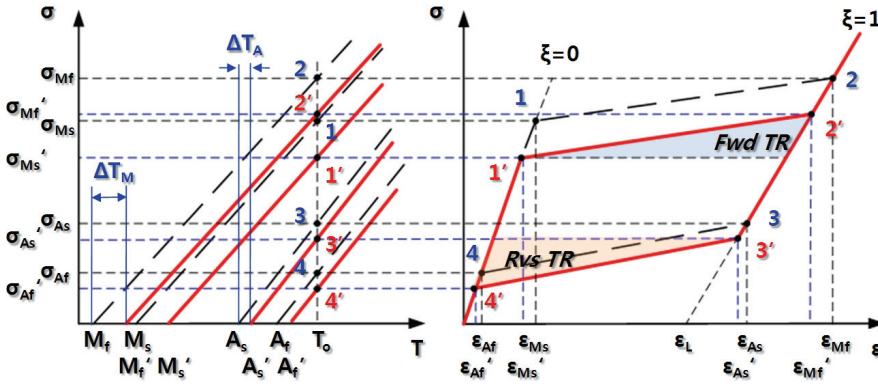


Figure 4: Modeling of trained behavior

By neglecting residual strain, trained stress-strain behavior can be regarded as the change of transformation temperatures in the phase diagram. Transformation bands move to right and the critical stresses are modified as:

$$\begin{aligned} \sigma'_{Ms} &= C_M(T_o - M'_s), \\ \sigma'_{Mf} &= C_M(T_o - M'_f), \\ \sigma'_{As} &= C_A(T_o - A'_s), \end{aligned}$$

and

$$\sigma'_{Af} = C_A(T_o - A'_f), \tag{15}$$

where

$$M'_s = M_s + \Delta T_M,$$

$$M'_f = M_f + \Delta T_M,$$

$$A'_s = A_s + \Delta T_A,$$

and

$$A'_f = A_f + \Delta T_A.$$

The changes of the transformation temperatures, ΔT_A and ΔT_M , can be determined by simple wire tests.

2.3 Strain Rate Dependent Behavior of SMA

SMA shows different behaviors according to the magnitude of the applied strain rate. Motahari et al. assumed the behavior of SMA under high strain rate to be an adiabatic process. In an adiabatic process, the transformation by external loads occurs within a very short time so that the latent heat hardly moves to the surroundings. As a result, the temperature of material is changed (Figure 5). When the transformation is completed, the critical stresses are [Motahari and Ghassemieh (2007)]

$$\sigma'_{Mf} = C_M(T_f - M_f),$$

$$\sigma'_{As} = C_A(T_f - A_s), \quad (16)$$

where

$$T_f \approx T_o \exp \left[-\frac{\Delta s_o}{c} \right] = C_{adi} T_o$$

T_f can be regarded as a material property calculated from the difference of specific entropies per unit volume for the martensite and austenite phase, $\rho \Delta s_o$, and specific heat per unit volume, ρc .

For the adiabatic process, the final temperature at the end of transformation is simplified as it is proportional to the initial temperature (Equation (16)). The specific heats at both phases are identical, since the composition is the same. Bo and Lagoudas et al. reported the methods to get $\rho \Delta s_o$ and we adopted $\rho c = 2.12 \text{ MJ/m}^3 \text{ K}$, $\rho \Delta s_o = -0.24 \text{ MJ/m}^3 \text{ K}$ for model correlation and numerical analysis in the following sections [Lagoudas and Bo (1999); Lagoudas and Entchev (2004)].

The behavior of the SMA material approaches an adiabatic process (segment 1-2', 3'-4) for very fast strain rate loading and it is different from the behavior for a quasi-static process (segment 1-2, 3-4). Tobushi, Shimeno, Hachisuka and Tanaka

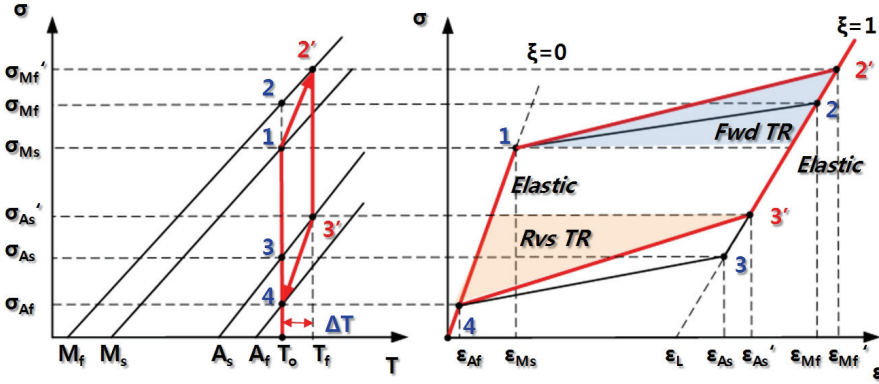


Figure 5: Modeling of adiabatic behavior

(1998); Dayananda and Rao (2008) conducted experimental research and found that the critical stress and strain rates are in a log function relation. Therefore, if we know the limit strain rate of quasi-static behavior ($\dot{\epsilon}_{sta}$) and the limit strain rate of adiabatic behavior ($\dot{\epsilon}_{adi}$), then the temperature increase for the intermediate strain rate can be interpolated using the weighting function, $W(\dot{\epsilon})$:

$$T_f = T_o + \Delta T, \tag{17}$$

where

$$\Delta T(\dot{\epsilon}) \approx (C_{adi} - 1)T_o W(\dot{\epsilon}),$$

$$W(\dot{\epsilon}) = \begin{cases} 0 & (\dot{\epsilon} < \dot{\epsilon}_{sta}) \\ \frac{\log(\dot{\epsilon}/\dot{\epsilon}_{sta})}{\log(\dot{\epsilon}_{adi}/\dot{\epsilon}_{sta})} & (\dot{\epsilon}_{sta} \leq \dot{\epsilon} \leq \dot{\epsilon}_{adi}) \\ 1 & (\dot{\epsilon} > \dot{\epsilon}_{adi}) \end{cases} \tag{18}$$

The limit strain rates are not only dependent on the diameter and length of the SMA wire but also on ambient temperature and the surrounding medium. Therefore, these values should be obtained by tests at conditions corresponding to those of the application. However, it is not easy to obtain appropriate test result for every situation. According to the work of Tobushi et al., NiTi wire shows quasi-static behavior below the strain rate of 2%/min [Tobushi, Shimeno, Hachisuka and Tanaka (1998)]. It was difficult to find the strain rate limit of adiabatic behavior for NiTi. As a result, we found the upper limit ($\dot{\epsilon}_{sta}$) inversely in section 3 using the wire test results with the strain rate above the lower limit and Equation (18).

3 Correlation with Test Data

Tensile tests of NiTi (Ni55.8wt%) wire were conducted according to ASTM2516. Tensile tests were carried out at various temperatures for $\phi=0.203\text{mm}$, $L=50\text{mm}$ wire specimens using UTM 5583 and a thermal chamber.

Figure 6 shows stress-strain curves at various temperatures. Plateau stresses increase as the temperature rises. Figure 7 shows phase transformation start and finish stresses with temperature. The fitted lines are the same as the transformation bands in Figure 1. The material properties are summarized in table 1.

Figure 8 shows the training effect for the same specimen by cyclic loads. The wire specimen was trained for 30 cycles at 6% maximum strain. As mentioned before, plateau stresses were decreased and irreversible residual strain was increased. Plateau stress during forward transformation at the virgin state was higher than fitted critical stress, using the data in Table 1.

Trained behavior is formulated by changes of transition temperatures (Equation (15)) in the engineering model and $\Delta T_M \cong 4^\circ\text{C}$, $\Delta T_A \cong 2^\circ\text{C}$ for 'N30' in Figure 8.

It is important to train SMA before using it in applications to make it work more stably. Tensile tests with different strain rates were conducted for the trained wire (30cycles, 6%max. strain). The test strain rates were $\dot{\epsilon} = 0.097/\text{sec}$, $\dot{\epsilon} = 0.001/\text{sec}$ (Figure 9). The test results show good agreement with those of the model when using the parameters $\dot{\epsilon}_{sta} = 3.33e - 4/\text{sec}$, $\dot{\epsilon}_{adi} = 0.333/\text{sec}$ (Equation (18)).

Table 1: Material Properties (NiTi(Ni55.8wt%))

Property	Value	Property	Value
D_A	42.4 GPa	Mf	-85°C
D_M	17.1 GPa	Ms	-80°C
C_A	6.3 MPa/ $^\circ\text{C}$	As	-25°C
C_M	4.9 MPa/ $^\circ\text{C}$	Af	-15°C
ϵ_L	0.04		

4 Vibration Analysis of Wire Damped Beam

We correlated model parameters in the previous section and this model was used for analyzing the responses of the SMA wire damped beam when equipped with a tip mass (200g) [Thomson, Balas and Leo (1995)]. The engineering SMA wire model was implemented as the user material subroutine (UMAT) of the Abaqus commercial finite element program.

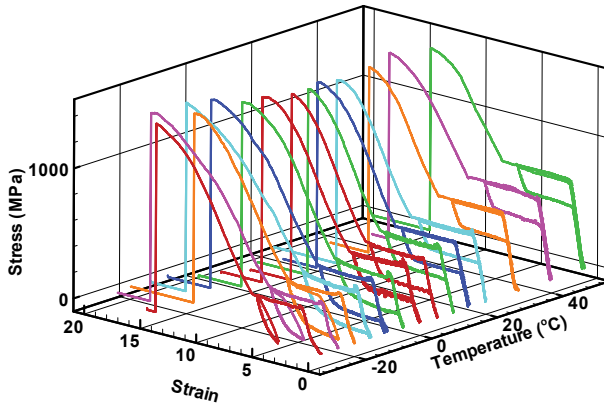


Figure 6: Stress-strain behavior with various temperatures (NiTi(Ni55.8wt%))

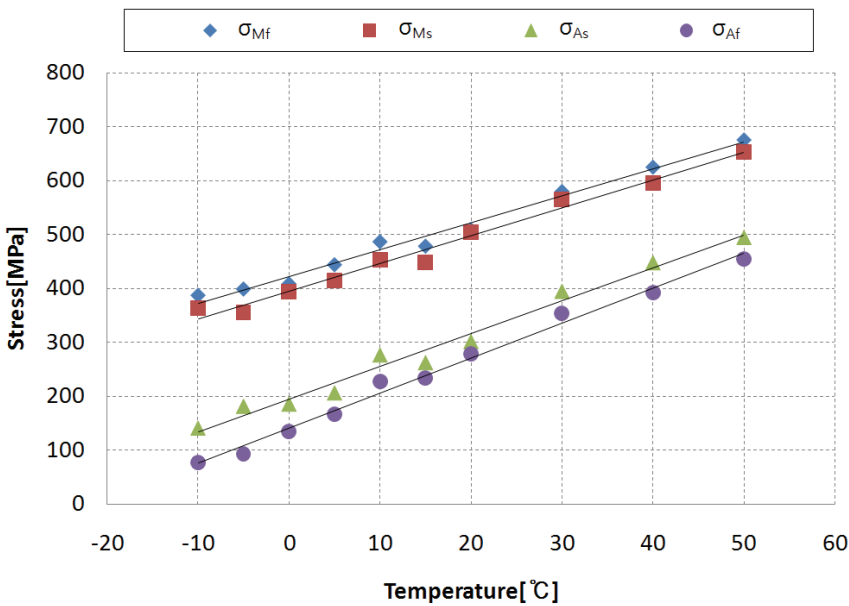


Figure 7: Critical stress - temperature diagram (NiTi(Ni55.8wt%))

The AL beam dimension is $327 \times 25.6 \times 4.9$ [mm³] and Young’s modulus is 69GPa. Trained SMA wires with the diameter 0.203mm were attached as in Figure 10. The angle between the AL beam and the SMA wire is 12.55°, and 1.58% pre-strain was applied to the SMA tendons using the ‘*Restart’ and ‘*Model change’ options in

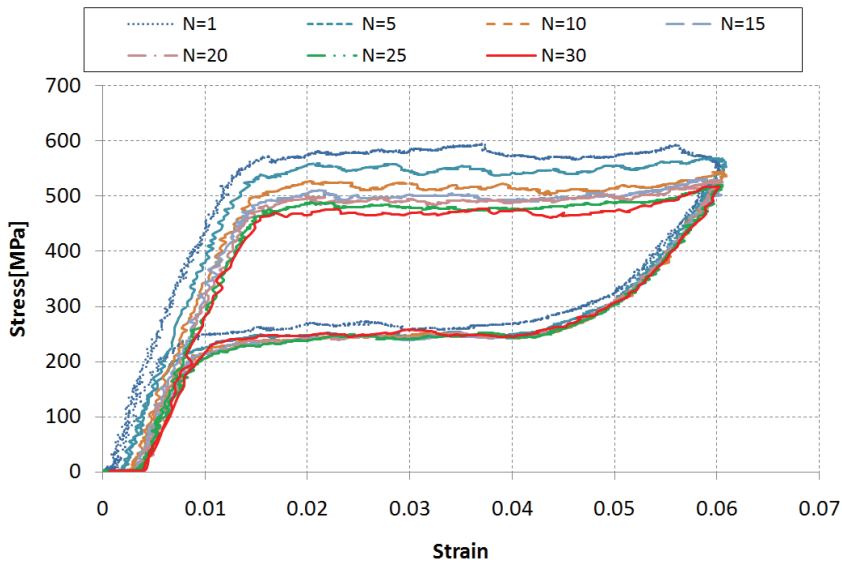


Figure 8: Training by cyclic loads (NiTi(Ni55.8wt%))

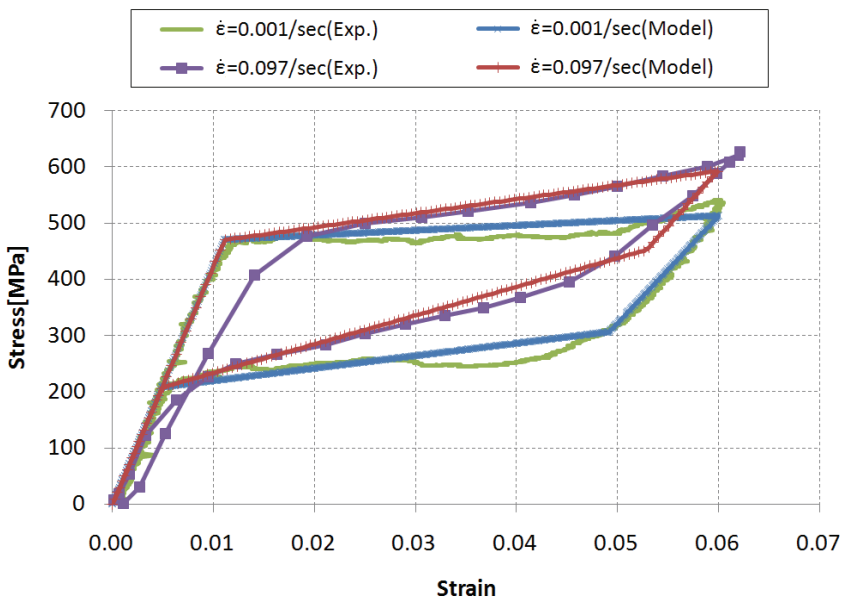


Figure 9: Model Correlation with Test Data(NiTi(Ni55.8wt%))

Abaqus. The fundamental frequency of the clamped beam is 11.7Hz.

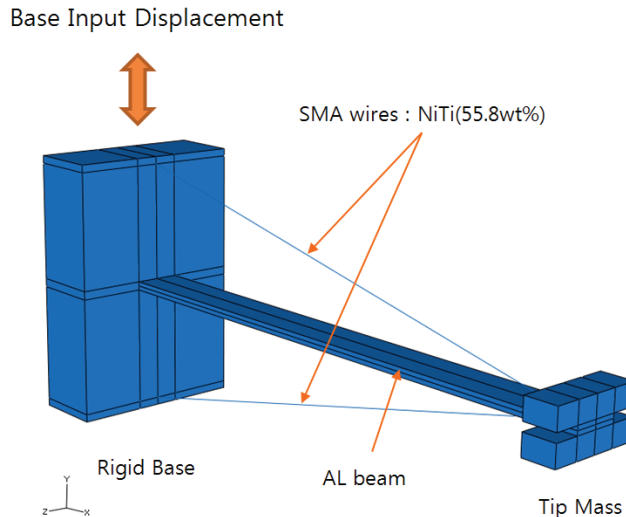


Figure 10: SMA wire damped beam

Sinusoidal displacement with 2mm amplitude and 5Hz frequency was applied on the rigid base. Tip displacements of the system with and without SMA wire were observed under base displacement inputs.

Figure 11 shows transverse displacements of the beam base and tip. The dynamic response of the beam tip is larger than the amplitude of the base. The maximum response of the wire damped beam is less than that of the beam without the wire.

Figure 12 shows corresponding stress-strain curves. 'Top' means the upper SMA wire, 'Btm' means the lower SMA wire in Figure 10. The strains are small since the change of the length of SMA wire is relatively small compared to its total length. Elastic responses are observed mainly in the vicinity of 1.58% pre-strain.

Sinusoidal displacement with 2mm amplitude and 11.7Hz frequency was applied on the rigid base. Although the SMA tendons do not actually exhibit a quasi-static behavior, quasi-static behavior was assumed for the SMA tendons here.

Figure 13 shows the transverse displacements. The base displacement and tip displacements are compared. ' A_o ' means the cross sectional area of the SMA wire for the diameter 0.203mm and ' $2A_o$ ' means twice the cross section area.

For the case with no wire, resonant response was present and transverse displacement diverged. The displacement in the case with SMA wire (A_o) increased quickly

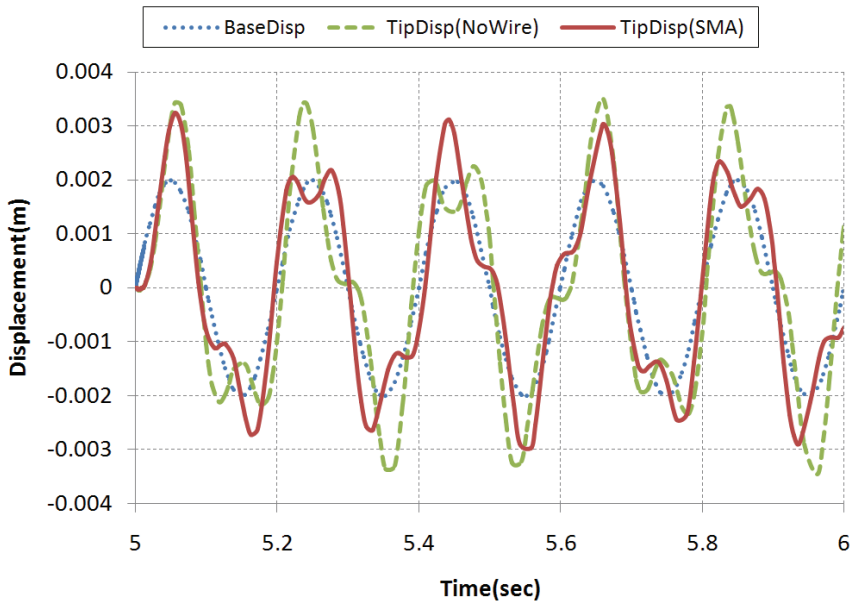


Figure 11: Tip displacements for base input (Amp=2mm, Freq=5Hz)

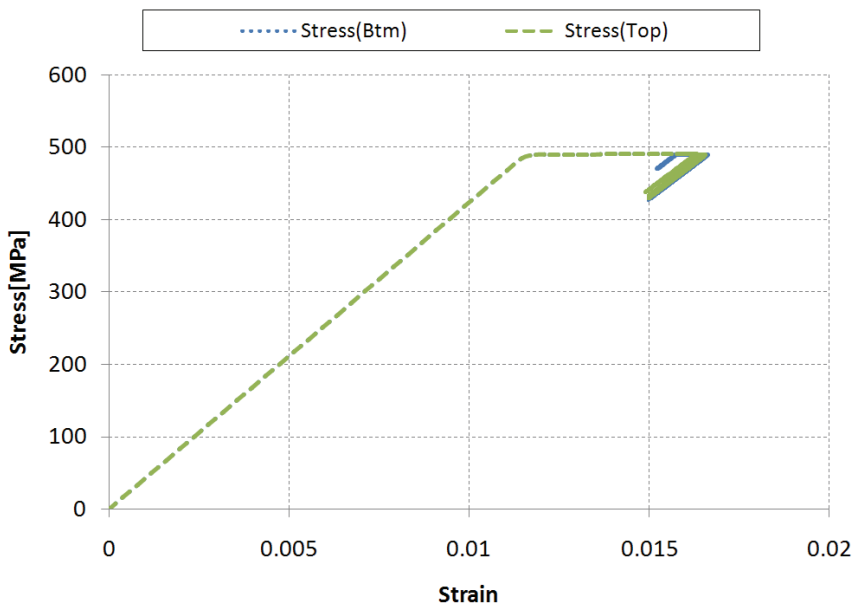


Figure 12: Stress-strain of SMA for base input (Amp=2mm, Freq=5Hz)

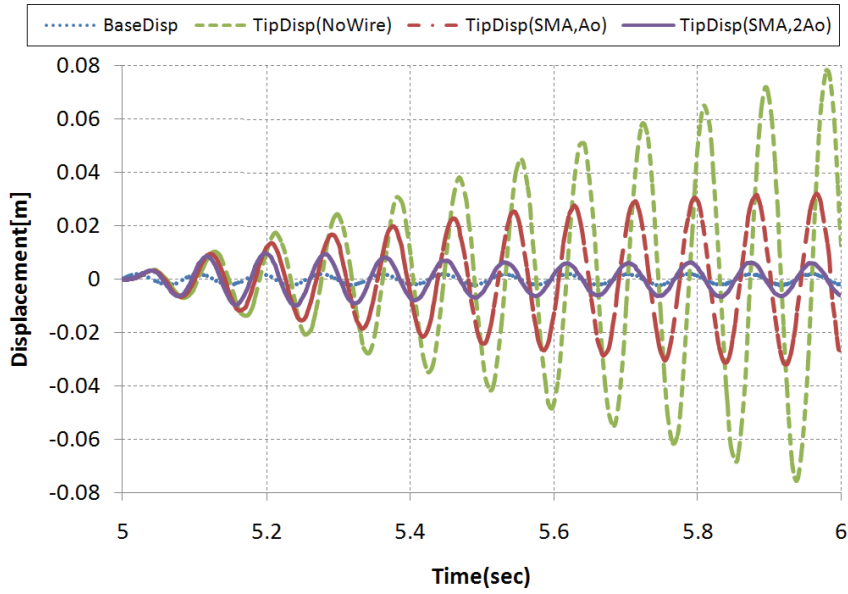


Figure 13: Tip displacements for base input (Amp=2mm, Freq=11.7Hz, Quasi-static)

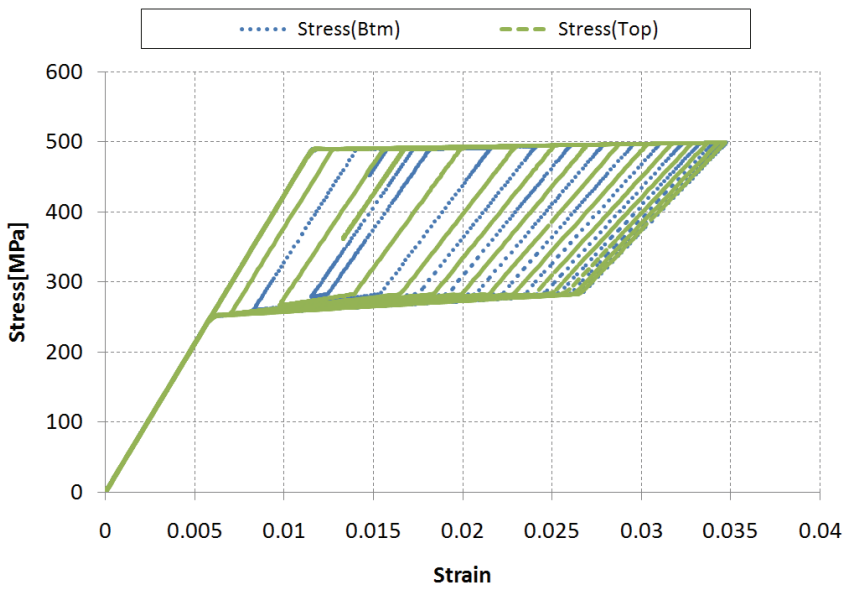


Figure 14: Stress-strain for base input (Amp=2mm, Freq=11.7Hz, Quasi-static, A_0)

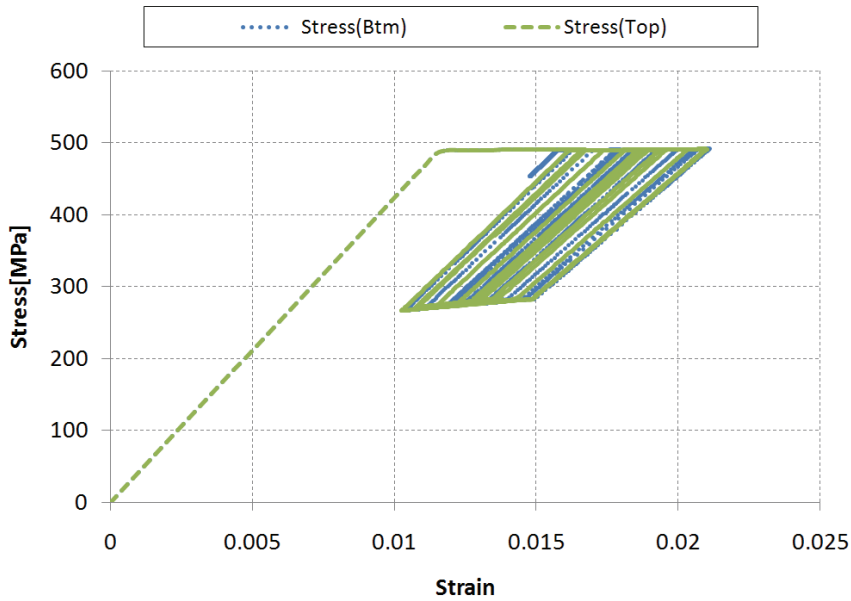


Figure 15: Stress-strain for base input (Amp=2mm, Freq=11.7Hz, Quasi-static, $2 A_0$)

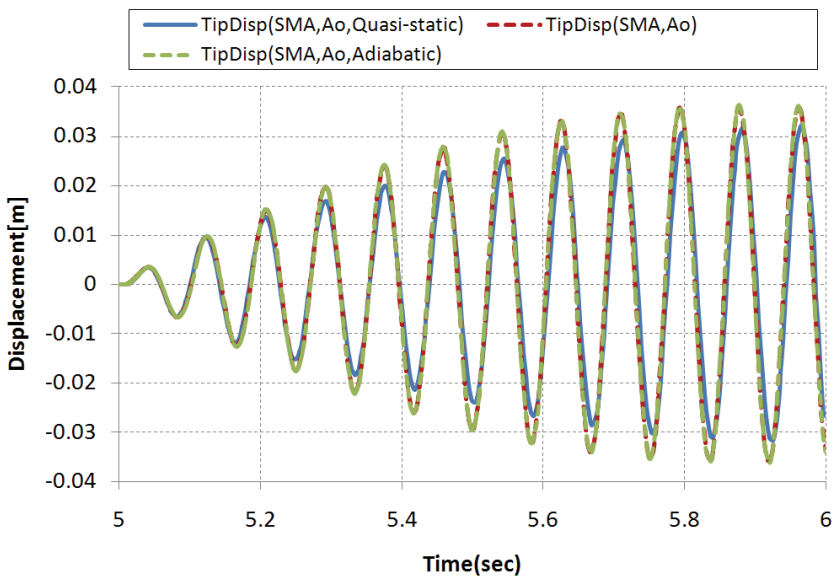


Figure 16: Tip displacements for base input (Amp=2mm, Freq=11.7Hz, A_0)

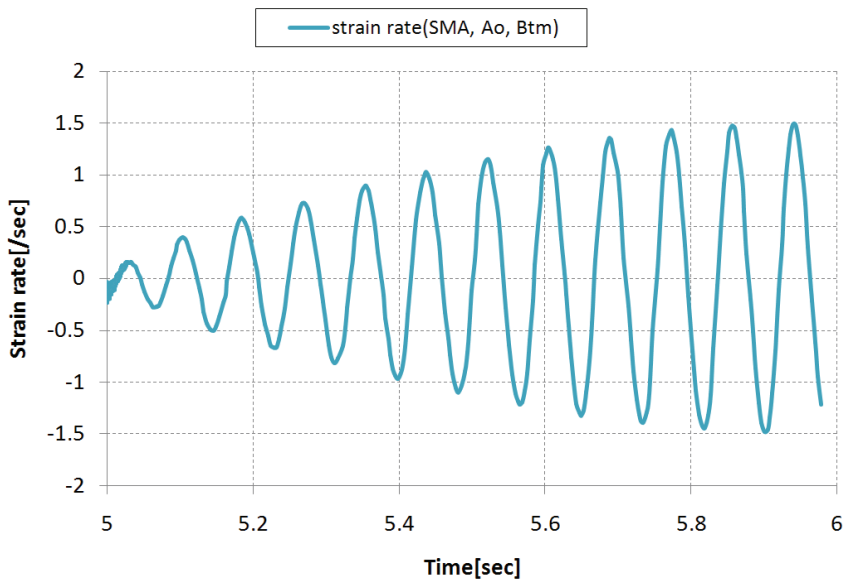


Figure 17: Strain rate for base input (Amp=2mm, Freq=11.7Hz, A_0)

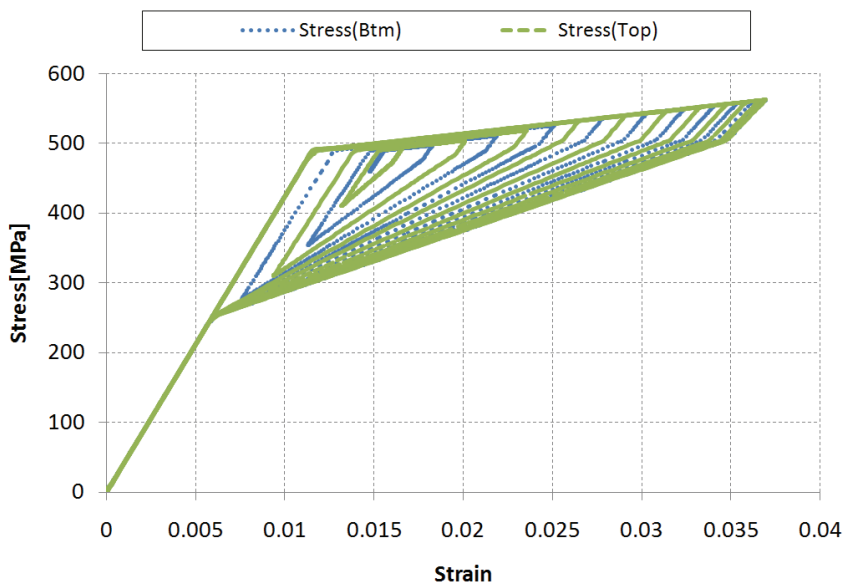


Figure 18: Stress-strain for base input (Amp=2mm, Freq=11.7Hz, Strain dependent, A_0)

at the beginning of the simulation and slowly in the rest of simulation. When the cross section area was doubled to increase the restraining force, limit cycle oscillation (LCO) occurred. The displacement of the tip increased up to 0.2sec from a shaking start ($t = 5.0\text{sec}$) and then decreased slightly.

Figures 14 and 15 show stress-strain curves for the SMA wires with ' A_o ' and with ' $2A_o$ ' respectively. The maximum strains of the SMA wire are about 3.5% for ' A_o ' and 2.1% for ' $2A_o$ '. Since the enclosed areas in the stress-strain curves correspond to the dissipated energy, it is considered that the former is more effective than the latter although the maximum amplitude of the tip displacement is larger for the former. Figure 16 shows the tip displacements considering strain rate dependent behaviors. Quasi-static and adiabatic processes are assumed for the purpose of comparison. The strain rate dependent model response is similar to the response of the adiabatic process. In this model, we set the strain rate limits as $\dot{\epsilon}_{adi} = 0.333/\text{sec}$ according to the correlation in Figure 9. Strain rates of the SMA wire (A_o) according to the base displacements are shown in Figure 17. The magnitude of the strain rate already exceeds the adiabatic limit after the first period. The tip displacement in the case of the quasi-static process is less than for the others. This result is more clearly explained by Figure 18, the stress-strain curve for the strain dependent model. The dissipated energy is much less than in the case of the quasi-static process (Figure 14).

5 Conclusions

An engineering model for SMA wire has been proposed in this study. In the model, the martensite volume fraction is used as an internal variable and the transformation kinetic is presented. The transformation kinetic is developed in terms of the strain conditions through the linear relation assumption of stress and strain, which is suitable for the conventional finite element method. Trained behavior by cyclic loads is considered in this simple model by using the properties for the stable trained state. Irreversible strain due to training is neglected and the resultant behavior is matched by changing the transformation temperatures. Strain rate dependent behavior is also modeled by interpolating the stress-strain responses of quasi-static and adiabatic processes. The parameters in the engineering model are correlated with the wire tests so that the model behaviors better reflect the actual wire motions. A numerical example for an SMA wire damped beam is presented to evaluate the effects of the strain rate dependence of SMA material. According to the analysis, the strain rate dependent behavior of SMA shows lower damping capacity when compared to the quasi-static behavior. The dynamic response of the system is also different from the case expected without considering strain rate dependent SMA behavior. Therefore, strain rate dependent SMA behavior should be accounted for

in vibration applications.

Acknowledgement: This research was supported by WCU(World Class University) program through the National Research Foundation of Korea funded by the Ministry of Education, Science and Technology, and by the second stage of the Brain Korea 21 Project in 2010.

References

Birman, V. (1997): Review of Mechanics of shape memory alloy structures, *Appl. Mech. Rev.*, Vol.50, No.11, Part.1, pp.629-645.

Brinson, L. C. (1993): One-Dimensional Constitutive Behavior of Shape Memory Alloys : Thermomechanical Derivation with Non-Constant Material Functions and Refined Martensite Internal Variable. *J. of Intell. Mater. Syst. And Struct.*, Vol. 4, pp. 229-242.

Dayananda, G. N.; Rao, M. S. (2008): Effect of strain rate on properties of superelastic NiTi thin wires. *Materials Science and Engineering A*, 486, pp. 96-103.

Dolce, M.; Cardone, D.; Marnetto, R. (2000): Implementation and testing of passive control devices based on shape memory alloys. *Earthquake Engng Struct. Dyn.*, Vol. 29 pp. 945-968.

Dolce, M.; Cardone, D. (2001): Mechanical behavior of shape memory alloys for seismic applications : 2. Austenite NiTi wires subjected to tension. *International Journal of Mechanical Sciences*, Vol. 43, pp. 2657-2677.

Jaber, M. B.; Smaoui, H.; Terriault, P. (2008): Finite element analysis of a shape memory alloy three-dimensional beam based on a finite strain description. *Smart Mater. Struct.*, Vol. 17, 045005.

Lagoudas, D. C.; Bo, Z. (1999): Thermomechanical modeling of polycrystalline SMAs under cyclic loading, PartII : material characterization and experimental results for a stable transformation cycle. *International Journal of Engineering Science*, Vol. 37, pp. 1141-1173.

Lagoudas, D. C.; Mayes, J. J.; Khan, M. M. (2001): Simplified Shape Memory Alloy (SMA) Material Model for Vibration Isolation. *Smart structures and materials: Modeling, signal processing, and control in smart structures Proc. SPIE*, Vol. 4326, pp. 452-461.

Lagoudas, D. C.; Ravi-Chandar, K.; Sarh, K.; Popov, P. (2003): Dynamic Loading of polycrystalline shape memory alloy rods. *Mechanics of Materials*, Vol. 35, pp. 689-716.

Lagoudas, D. C.; Entchev, P. B. (2004): Modeling of transformation-induced

plasticity and its effect on the behavior of porous shape memory alloys. Part I : constitutive model for fully dense SMAs. *Mechanics of Materials*, Vol. 36, pp. 865-892.

Liang, C.; Rogers, C. A. (1990): One-Dimensional Thermo- mechanical Constitutive Relations for Shape Memory Materials. *J. of Intell. Mater. Syst. And Struct.*, Vol. 1, pp. 207-235.

Liu, Y.; Xie, Z.; Humbeeck, J. V.; Delaey, L. (1998): Asymmetry of stress-strain curves under tension and compression for NiTi shape memory alloys. *Acta mater.*, Vol. 46, No. 12, pp. 4325-4338.

Motahari, S. A.; Ghassemieh, M. (2007): Multilinear one-dimensional shape memory material model for use in structural engineering application. *Engineering Structures*, Vol. 29, pp. 904-913.

Pelton, A. R.; Stöckel, D.; Duerig, T. W. (2000): Medical Uses of Nitinol. *Materials Science Forum*, Vols. 327-328, pp. 63-70.

Prahlad, H.; Chopra, I. (2003): Development of a Strain-rate Dependent Model for Uniaxial Loading of SMA Wires. *J. of Intell. Mater. Syst. And Struct.*, Vol. 14, pp. 429-442.

Qidwai, M. A.; Lagoudas, D. C. (2000): Numerical implementation of a shape memory alloy thermomechanical constitutive model using return mapping algorithms. *Int. J. Numer. Meth. Engng.*, Vol. 47, pp. 1123-1168.

Ren, W.; Li, H.; Song, G. (2007): Phenomenological modeling of the cyclic behavior of superelastic shape memory alloys. *Smart Mater. Struct.*, Vol. 16, pp. 1083-1089.

Rogers, C. A. (1990): Active vibration and structural acoustic control of shape memory alloy hybrid composites: Experimental results. *J. Acoust. Soc. Am.*, Vol. 88, Issue. 6, pp. 2803-2811.

Prahlad, H.; Chopra, I. (2001): Comparative Evaluation of Shape Memory alloy Constitutive Models with Experimental Data. *Journal of Intelligent Material Systems and Structures*, Vol. 12, pp. 383-395.

Saadat, S.; Noori, M.; Davoodi, H.; Hou, Z.; Suzuki Y.; Masuda, A. (2001): Using NiTi SMA tendons for vibration control of costal structures, *Smart Materials and Structures*, Vol 10, pp.695-704.

Tanaka, K.; Kobayashi, S.; Sato, Y. (1986): Thermomechanics of Transformation Pseudo-elasticity and Shape Memory Effect in Alloys. *International Journal of Plasticity*, Vol. 2, pp. 59-72.

Thomson, P.; Balas, G. J.; Leo P. H. (1995): The use of shape memory alloys for passive structural damping. *Smart Mater. Struct.*, Vol. 4, pp. 36-42.

Tobushi, H.; Shimeno, Y.; Hachisuka, T.; Tanaka, K. (1998) : Influence of strain rate on superelastic properties of TiNi shape memory alloy. *Mechanics of Materials*, Vol. 30, pp. 141-150.

Wang, X.; Xu, B.; Yue, Z. (2008): Phase transformation behavior of pseudoelastic NiTi shape memory alloys under large strain. *Journal of alloy and compounds*, Vol. 463, pp. 417-422.

